Supporting Information (SI) for

Defect-Seeded Atomic Layer Deposition of Metal Oxides on the Basal Plane of 2D Layered Materials

Michael F. Mazza,†‡ Miguel Cabán-Acevedo,†‡ Joshua D. Wiensch,† Annelise C. Thompson,† and Nathan S. Lewis†

†127-72, 210 Noyes Laboratory, Division of Chemistry and Chemical Engineering, California Institute of Technology, Pasadena, California 91125, United States

‡These authors contributed equally.

This material consists of full materials and methods section and Fig. S1-3.

Chemicals and Materials

Naturally occurring molybdenum disulfide (MoS_2) was purchased from 2D Semiconductors as well as from SPI supplies. Highly ordered pyrolytic graphite (HOPG) was purchased from SPI Supplies. Prior to deposition, samples were exfoliated multiple times with scotch tape (3M Company) or blue tape (Nitto Denko) to expose a pristine, flat surface. No difference in deposition patterning was observed resulting from use of different types of tape.

Atomic Layer Deposition

Titanium dioxide (TiO_2) and manganese oxide (MnO_x) were deposited using a Cambridge Nanotech S200 ALD system. All depositions were performed with 20 sccm of N_2 carrier gas at 150˚C at a base pressure of ~ 0.8 Torr. Tetrakis(dimethylamido)titanium (IV) (TDMAT, 99.999%

Sigma Aldrich) heated to 75 ˚C was used as the titanium precursor. 18.2 MΩ resistivity (Millipore) water at room temperature was used as the counter reactant. MnO_x was deposited from bis(ethylcyclopentadienyl)manganese ($(EtCp)_2Mn$ 98% STREM) heated to 95 ˚C.

In Figure 2, the ALD cycle consisted of a 0.015 s pulse of water, followed by a 0.1 s pulse of TDMAT. After each pulse, the chamber was evacuated for 20 s and 15 s respectively. The recipe in Figure 1 is the same except the TDMAT pulse time was adjusted from (a) 0.025 s, (b) 0.1 s, and (c) 0.4 s. A glass slide was placed under the flakes to monitor deposition conditions and growth-per-cycle.

In Figure 3, the recipes were optimized for pattern contrast according to the chemistry of each precursor and substrate. The sample shown in Figure 4a was generated using the same recipe as the sample in Figure 3a.

Figure 3a: 0.012 s(H_2O) – 15 s – 0.02 s(TDMAT) – 20 s

Figure 3b: 0.01 s(H_2O) – 15 s – 0.02 s(TDMAT) – 20 s

Figure 3c: 0.01 s(H_2O) – 30 s – 0.7 s($(EtCp)_2Mn$) – 30 s

Figure 3d: 0.007 s(H_2O) – 30 s – 0.6 s($(EtCp)_2Mn$) – 30 s

Scanning Electron Microscopy

Scanning electron microscopy (SEM) was performed using a FEI Nova NanoSE 450 at accelerating voltages of 3 and 5 keV with a 5 mm working distance.

Atomic Force Microscopy

Atomic force micrographs were collected using a Bruker Multimode 8 Atomic Force Microscope in air. Scans were collected in ScanAsyst mode using SiN tips with a nominal spring constant of 0.4 N m^{-1}.

Ellipsometry

Ellipsometry was performed on the glass slides that were placed beneath the MoS_2 substrate. The data were fit according to a simple model of an absorbing oxide on glass.

Transmission Electron Microscopy

Multilayer MoS_2 TEM samples were prepared by mechanical exfoliation of commercial bulk single crystals using blue tape (Nitto Denko) followed by gentle dry transfer of the exfoliated flakes onto a TEM grid (C-Flat Holey Carbon 1.2/1.3um 200 mesh copper grid from Electron Microscopy Sciences). Transmission electron microscopy (TEM) data were collected using a FEI Tecnai Polara (F30) TEM at an accelerating voltage of 200 keV.

Determination of Film Thickness.

Atomic force microscopy data gathered on an exfoliated MoS_2 crystal patterned with 1000 cycles of TiO_2 yielded a height difference between the deposited regions and the opposite-facing interior of ~ 53 nm (Figure S1). This value is in good agreement with ellipsometric data that yielded a film thickness of 55 nm. At 150 ˚C, the generally accepted growth-per-cycle for ALD of TiO_2 from TDMAT and H_2O is 0.52 Å $cycle^{-1}$.[1] The data thus strongly suggest that the opposite-facing, unreacted triangles are the basal plane of the MoS_2 substrate. Given the excellent agreement between the ellipsometry data and the AFM results, ellipsometry was used to determine the film thickness and GPC for all the conditions presented in Figure 1.

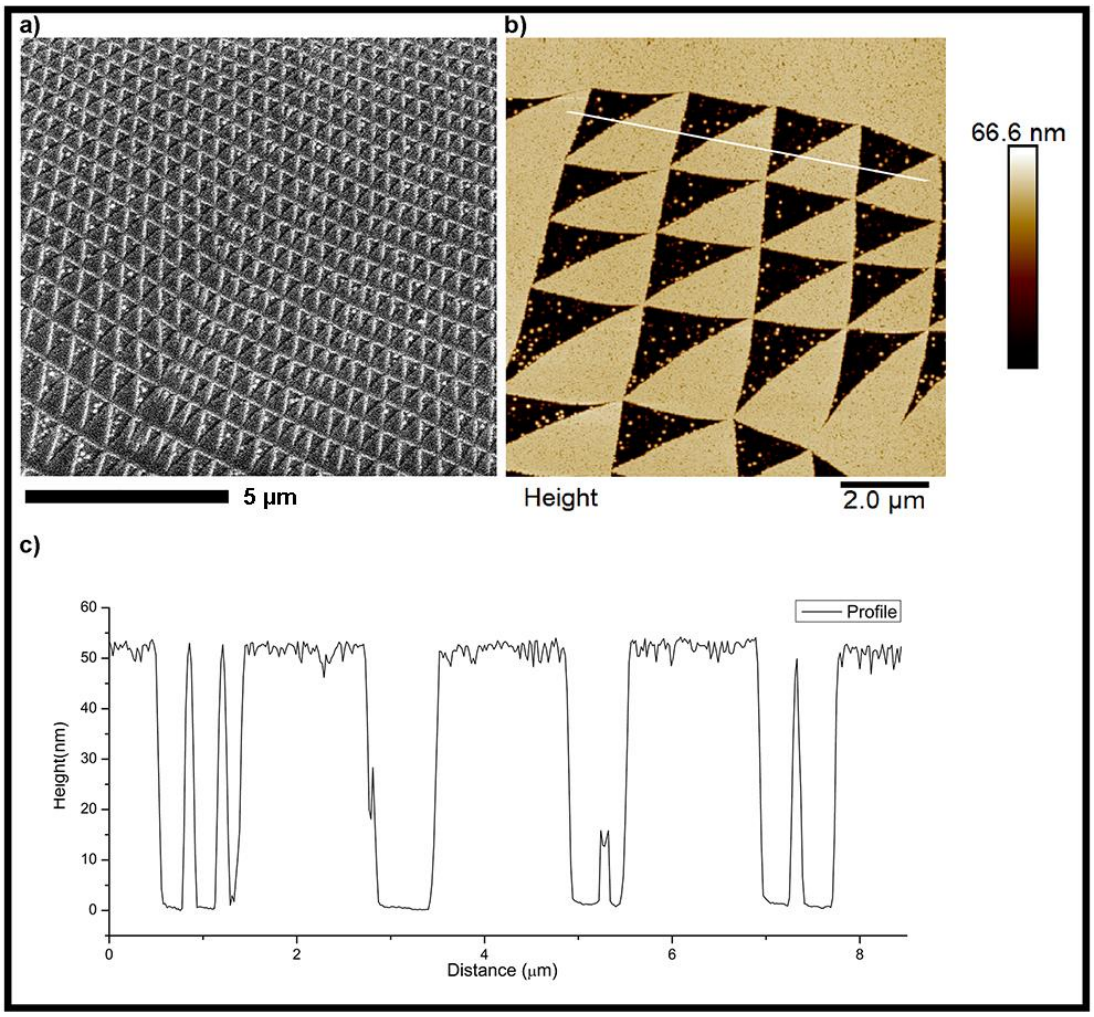

Figure S1. SEM image of a highly ordered, patterned area on exfoliated MoS_2 after 1000 cycles of TiO_2 (a). AFM image of a different region on the same sample (b). Height profile of the AFM image across the white line (c).

Deposition Behavior Investigated through Microscopy

SEM, AFM, and optical microscopy were performed on an exfoliated MoS_2 crystal patterned with 800 cycles of TiO_2 at a higher supersaturation condition than the sample shown in Figure S1. AFM and SEM were performed at mutually the same location on the sample (Figure S2c, S2d) to show that the film composition, thickness, and packing density are responsible for the SEM contrast shown throughout the main text. This deposition behavior was further confirmed with

optical microscopy (Figure S2b) that showed contrast having the same pattern as the SEM and AFM conditions. The yellow regions in the optical image showed a thin film of TiO_2 on MoS_2 with the white regions corresponding to the opposite-facing triangular interiors with nanoparticle aggregates.

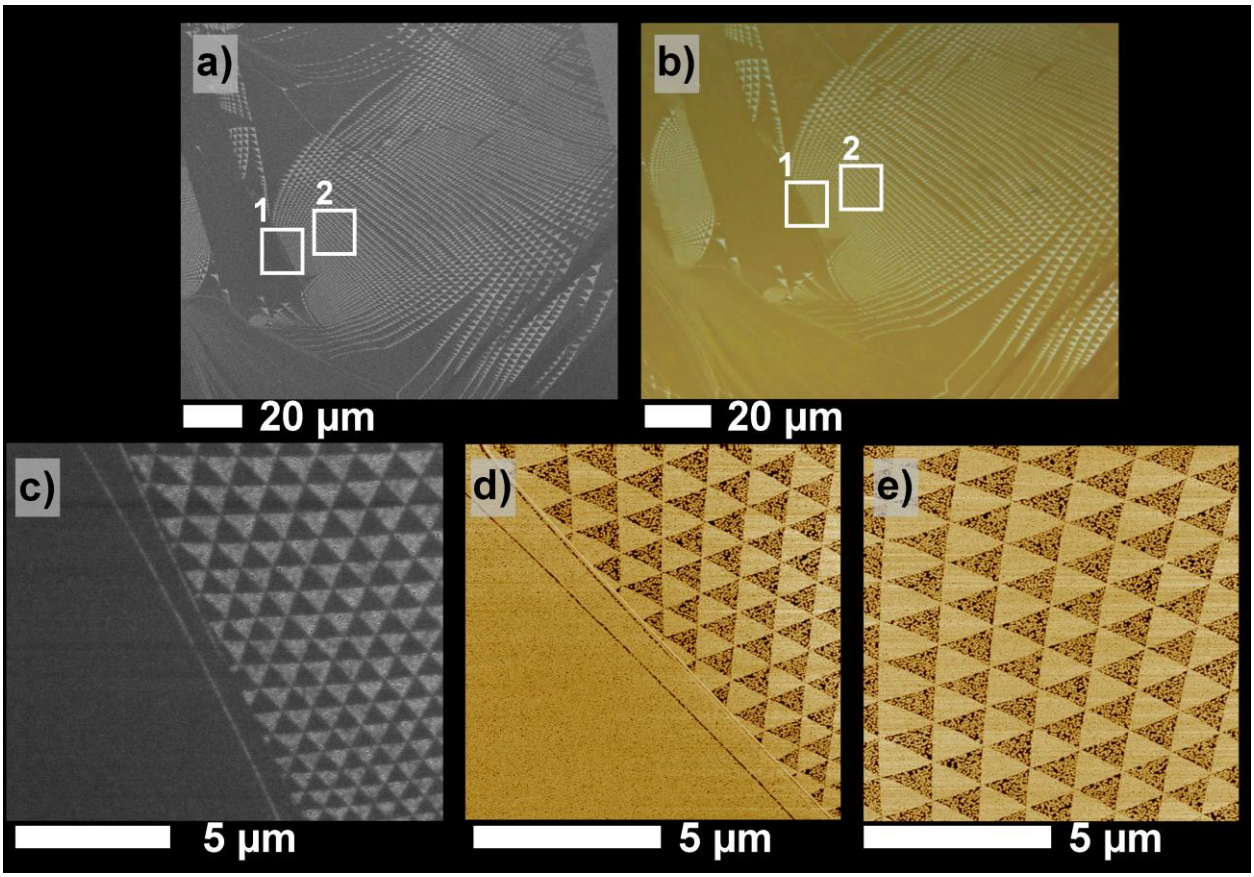

Figure S2. SEM image of highly ordered patterned area on MoS_2 after 800 cycles of TDMAT and H_2O (a). Optical microscope image of the same area (b). Close up SEM image of the region indicated in box 1 (c). Close up AFM image of the same region indicated in box 1(d). AFM image of the highly-ordered patterned region in box 2(e).

Dislocation Networks and Extended Nodes.

Translational or rotational disruptions to the Van der Waals stacking of layers on 2D materials can result in the formation of dislocation networks. In networks composed of three distinct undissociated dislocations with Burgers vectors **PQ**, **RP**, and **RQ** (Figure S3a), interactions between dislocations can result in the formation of double contrast due to multiple Bragg reflections being satisfied. Figure S3b shows an interaction network with lines A and B formed by contrast involving two Bragg reflections simultaneously. A crossing point which enables the preservation of the relative position of the A and B lines throughout the network is observed at node 1 (N1), node 3 (N3), and node 5 (N5). However, in naturally occurring MoS_2 (molybdenite), interaction networks without visible crossing points have been observed under TEM, as schematically shown in Figure S3c.[2,3] The absence of crossing points results in an apparent change in the relative position of the A and B lines between the segments N1 to N3 and N3 to N5, resulting in an apparent break in symmetry. It has been proposed that such segments are still present but are simply not visible due to the presence of extinction contours.[3] Figure 4d,e of the main manuscript shows observed interaction networks of the type shown in Figure S3c for mechanically exfoliated MoS_2.

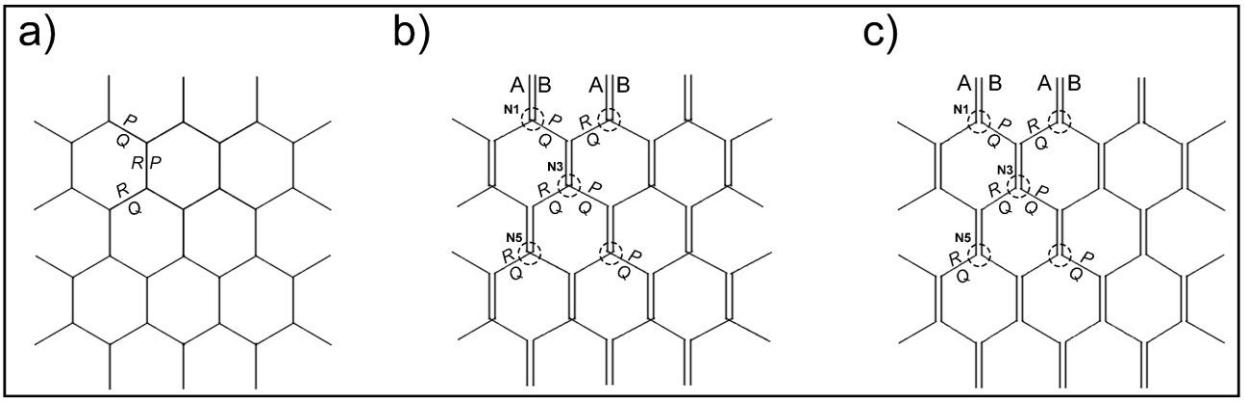

Figure S3. (a) Dislocation network composed of three undissociated dislocations with Burgers vectors **PQ**, **RP**, and **RQ**. (b) Interaction network with crossing points. (c) Interaction networks without visible crossing points.

Concave Triangular Voids

AFM characterization was conducted to demonstrate that in some cases empty triangular voids with concave side walls and convex triangular deposits were also observed. Since a crystal solid can reduce the total stacking fault energy by curving partial dislocation lines towards the stacking fault region, the observation of triangles with concave side walls is indicative of an extended stacking fault node. [5,6] The observation of concave triangular voids after deposition suggests that in some cases the extended stacking fault nodes appear to be less reactive than the pristine surface.

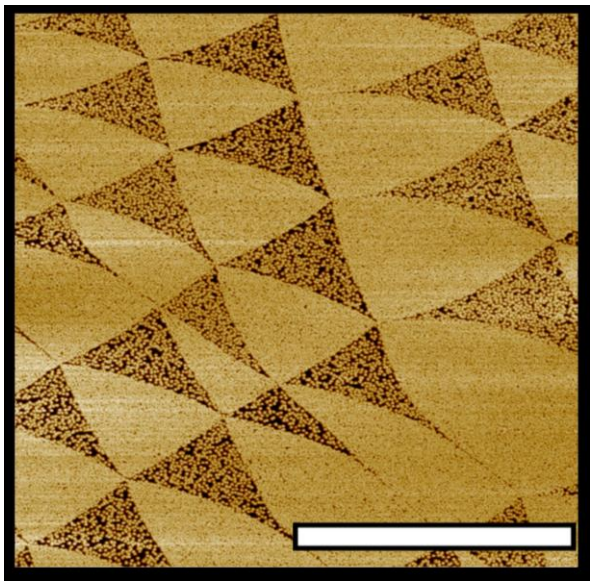

Figure S4. AFM data showing convex triangular deposits neighboring concave triangular voids. Nanoparticles are randomly distributed in the interior of the voids. Scale bar is 5 μm.

REFERENCES:

1. Abendroth, B.; Moebus, T.; Rentrop, S.; Strohmeyer, R.; Vinnichenko, M.; Weling, T.; Stöcker, H.; Meyer, D. C. Atomic Layer Deposition of TiO_2 from Tetrakis(Dimethylamino)Titanium and H_2O. *Thin Solid Films* **2013**, *545*, 176–182.

2. Hörl, E. M. Dislocations in Molybdenite. *Journal of Applied Physics* **1965**, *36* (1), 253–261.

3. Kamiya, Y.; Ando, K.; Nonoyama, M.; Uyeda, R. Dislocation Networks and Moiré Patterns of Molybdenite. *J. Phys. Soc. Jpn.* **1960**, *15* (11), 2025–2035.

4. Takahashi, N.; Shiojiri, M.; Enomoto, S. High Resolution Transmission Electron Microscope Observation of Stacking Faults of Molybdenum Disulphide in Relation to Lubrication. *Wear* **1991**, *146* (1), 107–123.

5. Yadav, S. K.; Shao, S.; Wang, J.; Liu, X.-Y. Structural Modifications Due to Interface Chemistry at Metal-Nitride Interfaces. *Scientific Reports* **2015**, *5* (1), 17380.

6. Dai, S.; Xiang, Y.; Srolovitz, D. J. Structure and Energy of (111) Low-Angle Twist Boundaries in Al, Cu and Ni. *Acta Materialia* **2013**, *61* (4), 1327–1337.